DOI: 10.61782/fa.2025.0681

FORUM ACUSTICUM EURONOISE 2025

Piezoelectric MEMS Temperature Sensor based on Acoustic Flexural Plate Waves

Stefano Bertelli[1*] **Alessandro Nastro**[1] **Marco Baù**[1] **Marco Ferrari**[1]
Libor Rufer[2] **Skandar Basrour**[3] **Vittorio Ferrari**[1]
[1] Department of Information Engineering, University of Brescia, 25123, Brescia, Italy
[2] ADT MEMS, France
[3] Univ. Grenoble Alpes, CNRS, Grenoble INP*, TIMA, 38000 Grenoble, France

ABSTRACT

Piezoelectric sensors based on acoustic waves propagating into micro electro-mechanical systems (MEMS) are a lively research area, with devices based on flexural plate waves (FPW) finding applications across various fields, including industrial and biological sectors. In this paper, a temperature sensor based on a piezoelectric MEMS that exploits the first antisymmetric mode, denoted as the A_0 or FPW mode, of Lamb waves generated in a diaphragm is presented. The micromachined diaphragm is composed of a stack of doped silicon and an aluminum nitride (AlN) piezoelectric layer with aluminum interdigital transducers (IDTs) employed for wave generation and detection. The proposed MEMS sensor exploits the variation of the FPW propagation velocity in the diaphragm due to temperature. The sensor expected working temperature range is at least 20 to 80 °C and in this preliminary phase has been tested from 25 to 45 °C by means of a tailored PID controlled temperature chamber including a Peltier cell and a Pt100 sensor while measuring the electrical admittance of a single IDT. The working principle has been validated within the frequency range from 11.185 to 12.88 MHz. Measurements have confirmed the sensor working principle, demonstrating a sensitivity of -426.5 Hz/°C and highlighting its potential for extending the operating temperature range.

Keywords: *Lamb waves, MEMS, piezoelectric, temperature sensor.*

[*] ***Corresponding author***: *stefano.bertelli@unibs.it.*

1. INTRODUCTION

MEMS-based sensors are extensively employed in several research fields [1], including environmental monitoring [2], biomedical diagnostics [3], and industrial automation [4]. MEMS temperature sensors play a critical role in various applications where precise temperature monitoring is essential, such as tracking the internal temperature of smartphones [5], measuring human body temperature [6], or regulating indoor environments in heating, ventilation, and air conditioning (HVAC) systems [7]. Given the widespread adoption of MEMS temperature sensors, significant efforts have been made to develop and optimize different transduction principles, including resistive [8], optical [9], and piezoelectric [10], the latter being particularly notable for its high responsivity to temperature variations and suitability for harsh environments [10]. Specifically, among piezoelectric sensors, acoustic wave-based sensors have gained attention due to their high sensitivity and reliability [11]. Typically, acoustic wave MEMS temperature sensors are based on surface acoustic wave (SAW) [12], bulk acoustic wave (BAW) [13], and flexural plate wave (FPW) [14]. Among acoustic wave sensors, FPW MEMS exploit the propagation of Lamb waves in thin diaphragms and exhibit several advantages, including the operating frequency range typically in the tens of MHz and the ability to operate in contact with liquids with low losses [15,16]. In this context, this work presents a novel piezoelectric MEMS temperature sensor based on flexural plate waves, specifically exploiting the first antisymmetric mode (A_0) of Lamb waves. The sensor exploits the variation in the propagation velocity of FPWs in a micromachined piezoelectric diaphragm as a function of temperature, enabling thermal measurements.

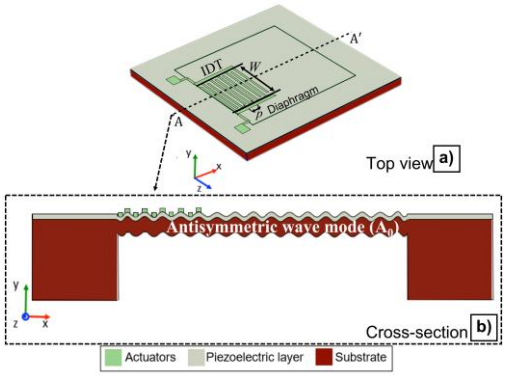

Figure 1. Top (a) and cross-section (b) schematic views of the proposed piezoelectric temperature sensor.

2. DESCRIPTION AND WORKING PRINCIPLE OF THE PROPOSED MEMS TEMPERATURE SENSOR

Fig. 1a shows a schematic representation of the top view of the proposed MEMS. The device is composed of a square diaphragm with an interdigital transducer (IDT), positioned close to the edge of the diaphragm, which comprises two interleaved comb-shaped electrodes. Each electrode consists of equally spaced fingers with a pitch p and aperture W, located on top of a piezoelectric layer. By applying a sinusoidal voltage across the IDT fingers, a perturbation in the thickness of the AlN layer, and consequently in the diaphragm, is induced, as schematically shown in the cross-section view A-A' of Fig. 1b. At specific frequencies, this perturbation induces mechanical vibrations in the diaphragm in the form of Lamb waves. Specifically, the first antisymmetric mode (A_0) has been excited at the synchronous frequency $f_{A0}=v_{A0}/p$ where v_{A0} represents the propagation velocity of the A_0 mode. The proposed MEMS has been manufactured by means of the PiezoMUMPs process [17]. The device features overall dimensions of 9 mm × 9 mm and incorporates a 6 mm × 6 mm squared composite diaphragm. The top and bottom views of the manufactured device are shown in Fig. 2a and 2b, respectively. The diaphragm consists of a material stack composed of a 10 µm thick silicon (Si) layer and a 0.5 µm thick piezoelectric aluminum nitride layer. The AlN layer on the composite diaphragm can be actuated by eight IDTs, positioned on the inner and outer edges of the diaphragm and arranged symmetrically with respect to its center.

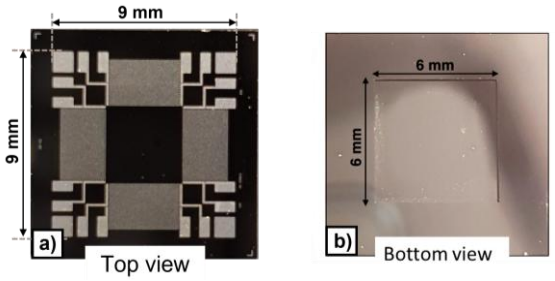

Figure 2. Top (a) and bottom (b) views of the fabricated piezoelectric MEMS sensor.

Each IDT comprises two interleaved comb-shaped electrodes. Each electrode consists of $N = 10$ equally spaced fingers, with a pitch $p = 112$ µm and an aperture $W = 3.5$ mm. By considering the tolerances of the fabrication process the frequency f_{A0} is expected to be between 11 and 15 MHz [15]. The proposed MEMS sensor exploits the variation of the FPW propagation velocity v_{A0} in the diaphragm due to thermal expansion and changes in the Young's modulus of the materials as a function of temperature [18,19]. The device was configured as a one-port transducer and the electrical admittance $G(f)$ of a single IDT has been analyzed as a function of temperature. This is expected to produce a frequency shift in the IDT admittance pattern centered at f_{A0} of the A_0 mode [14, 20], with a downshift in frequency as the temperature increases. The expected working temperature range is at least 20 to 80 °C as observed in similar AlN-based MEMS devices, [21] while in this preliminary phase it has been tested within 25 and 45 °C.

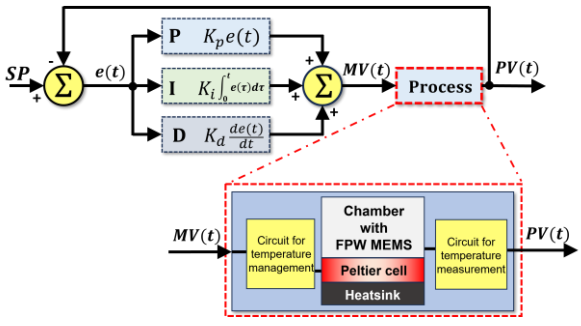

Figure 3. Schematic representation of the implemented PID controller. The enlarged view shows a detail of the controlled process, embedding the FPW MEMS temperature sensor, the actuator (Peltier cell), and auxiliary circuits.

3. EXPERIMENTAL SETUP

The operating principle was experimentally investigated using an HP4194A impedance analyzer and a custom experimental setup, including a thermal chamber regulated by a proportional-integral-derivative (PID) controller. Fig. 3 shows the block diagram of the implemented PID controller. The time-dependent process variable *PV(t)* corresponds to the chamber temperature *T*, which is measured using a dedicated temperature sensing circuit and compared with the setpoint variable *SP*, representing the desired operating temperature. The error $e(t) = SP - PV(t)$ is processed by the PID control algorithm, which incorporates proportional, integral, and derivative control actions with gains K_p, K_i, and K_d, respectively. The resulting manipulated variable *MV(t)* feeds a thermal management circuit to control the chamber temperature *T*. The system is specifically designed to establish and maintain predefined temperature profiles, enabling a precise characterization of the proposed MEMS temperature sensor. Fig. 4a illustrates the developed thermal chamber, which has been built using insulating foam layers. A Marlow TG12-6 Peltier cell has been employed as the heating element and is positioned at the bottom of the chamber, with a heat sink attached to its outer surface as shown in Fig. 4b. The Peltier cell is driven by a Pulse-Width Modulation (PWM) controller, which facilitates power regulation.

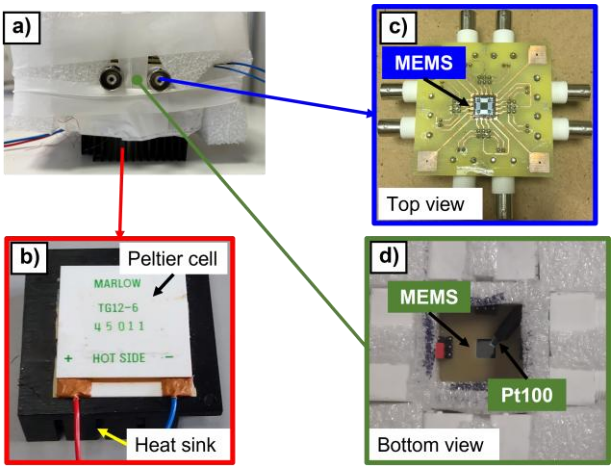

Figure 4. Experimental setup. Thermal chamber made of insulating foam (a). Peltier cell and the heat sink used to control the chamber temperature (b). Top view of the PCB adapter for the proposed MEMS sensor (c). Bottom view of the PCB adapter and Pt100 reference sensor positioned inside the chamber (d).

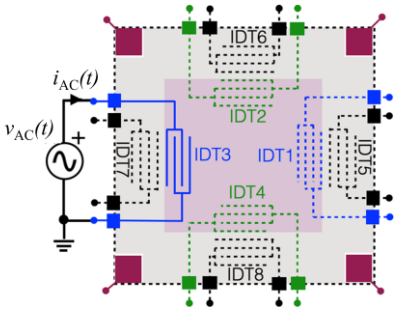

Figure 5. Simplified schematic representation of the proposed MEMS sensor configured for electrical admittance measurements.

The PWM driver is controlled via the PID algorithm, implemented through a LabVIEW interface. The chamber temperature *T* is measured using an HP34401A multimeter connected to a Pt100 resistive temperature detector (RTD) temperature sensor located inside the chamber, with a sampling time of 1 s. The FPW MEMS temperature sensor was fixed on a printed circuit board, as shown in Fig. 4c and Fig. 4d.

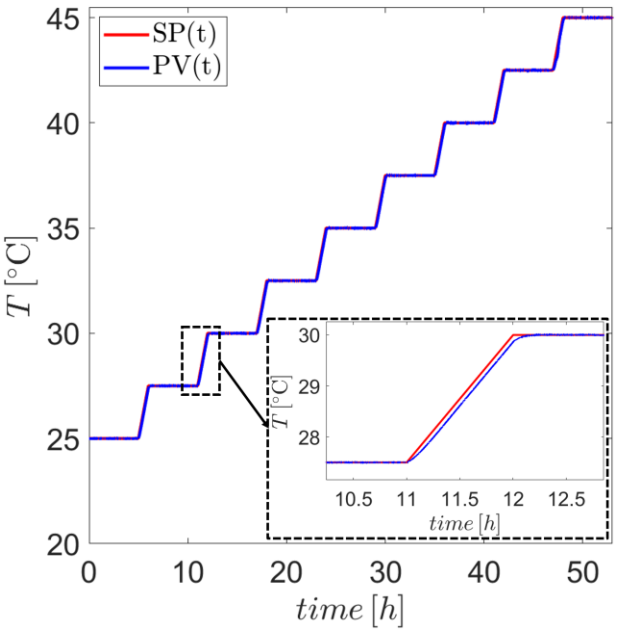

Figure 6. Setpoint (*SP*) and measured chamber temperature (*PV*) as a function of time. The inset shows the transient response to a heating step of 2.5 °C.

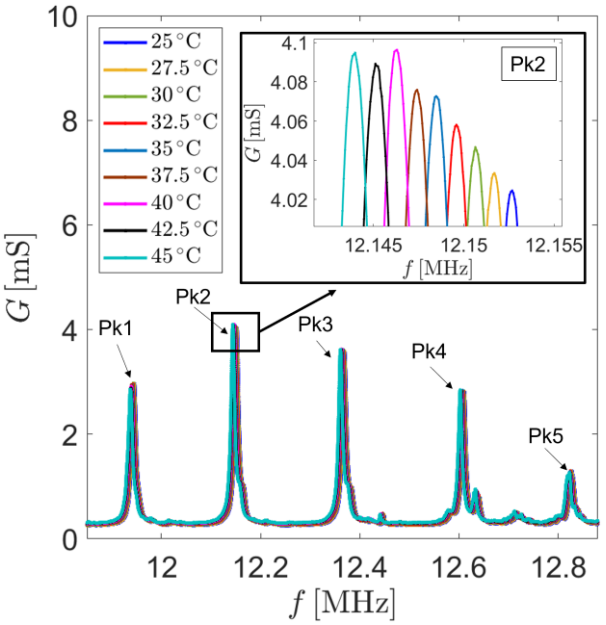

Figure 7. Measured conductance *G(f)* of a single IDT as a function of the excitation frequency *f* at different temperature *T*. The inset shows an enlarged view of the second peak Pk2 of *G(f)* at different temperatures.

4. EXPERIMENTAL RESULTS

To validate the proposed MEMS temperature sensor, the electrical conductance *G(f)* of a single IDT, namely IDT3, was measured according to the schematic diagram shown in Fig. 5, while the remaining IDTs were left floating, i.e., electrically unconnected. A sinusoidal excitation with a rms amplitude V_{AC} of 1 V was applied, while the frequency *f* was swept between 11.185 and 12.88 MHz with a step size of 70 Hz at different temperatures. The proposed sensor has been tested within the temperature range of 25°C to 45°C, while varying the setpoint *SP* with a 2.5°C step as shown in Fig. 6. The time required to achieve steady state after each 2.5°C step was set as 1 hour, as illustrated in the inset of Fig. 6. An additional delay of 30 minutes after the beginning of the steady state was introduced before conducting admittance measurements. Thanks to the continuous real-time temperature control implemented via the PID, the *PV* accurately followed the *SP* ensuring precise thermal regulation, as shown in the inset of Fig. 6. Measurements were performed while maintaining a stable temperature over time, with a variation of approximately ±0.02 °C. Fig. 7 shows the measured *G(f)* of IDT3 as a function of the excitation frequency *f*. The obtained conductance patterns show five distinctive main peaks within the considered bandwidth caused by the IDT3 location on the diaphragm and by the diaphragm dimensions [15, 22]. A conductance peak is obtained when the wavelength is an integer submultiple of the propagation path, defined as twice the distance between the center of the IDT and the outermost constraint of the diaphragm [22]. The obtained series of peaks (Pk1-5) exhibits a rigid downshift in frequency as the temperature *T* increases, as visible in the inset of Fig. 7, where the second peak of *G(f)* is shown. Fig. 8 illustrates the frequency shifts Δf as a function of ΔT, where $\Delta T = T - T_0$ with T_0 = 25 °C. The frequency shift is defined as $\Delta f = f_m - f_{m0}$, where f_m represents the frequency at which the conductance *G(f)* reaches its maximum for the five measured conductance peaks, and f_{m0} the corresponding values at the reference temperature T_0. The dashed line represents the linear fitting of the average frequency shifts obtained by averaging the individual shifts of the conductance peaks as a function of ΔT. For ΔT = 25 °C, a frequency variation of -8.628 kHz has been measured. The proposed MEMS sensor exhibits a sensitivity of -426.5 Hz/°C, with a maximum nonlinearity error, referred to the full scale, of 1.18%.

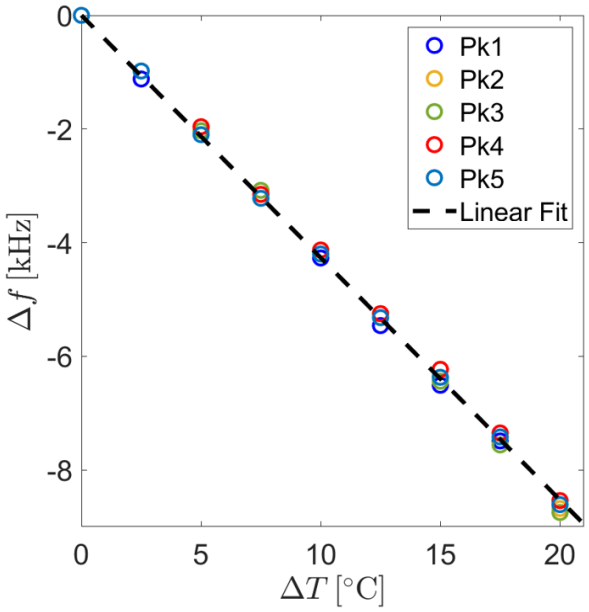

Figure 8. Frequency shifts Δf as a function of ΔT for the five conductance peaks. The dashed line represents the linear fit of the average frequency shifts obtained for the five peaks.

5. CONCLUSIONS

In this work, a piezoelectric FPW MEMS temperature sensor was presented. The proposed sensor exploits the first antisymmetric (A_0) vibration mode of Lamb waves to measure the surrounding temperature. The operating principle was experimentally validated using a custom PID-controlled temperature chamber, ensuring precise measurement conditions, accurate characterization, and minimal external interferences. The sensor was validated over the temperature range of 25 °C to 45 °C within the 11.185 to 12.88 MHz frequency range. For ΔT = 25 °C, a frequency shift of -8.628 kHz was measured. The proposed MEMS sensor exhibits a sensitivity of -426.5 Hz/°C with a maximum nonlinearity error of 1.18% referred to the full scale. The results obtained demonstrate the feasibility of using FPW-based piezoelectric MEMS for temperature sensing applications, confirming the expected downshift in frequency of the conductance pattern as the temperature increases and highlighting its potential to operate over an extended temperature range.

6. ACKNOWLEDGMENTS

The work has been carried out within the research project funded by the European Union NextGenerationEU.

7. REFERENCES

[1] J. Bryzek, S. Roundy, B. Bircumshaw, C. Chung, K. Castellino, J. Stetter and M. Vestel, "Marvelous MEMs," *IEEE Circuits and Devices Magazine*, vol. 22, no. 2, pp. 8–28, Mar. 2006, doi: 10.1109/MCD.2006.1615241.

[2] S. E. Moon, N. J. Choi, H. K. Lee, J. Lee, and W. S. Yang, "Semiconductor-type MEMS gas sensor for real-time environmental monitoring applications," ETRI Journal, vol. 35, no. 4, pp. 617–624, Aug. 2013, doi: 10.4218/etrij.13.1912.0008.

[3] K. Menon, R. A. Joy, N. Sood, and R. K. Mittal, "The Applications of BioMEMS in Diagnosis, Cell Biology, and Therapy: A Review," Bionanoscience, vol. 3, no. 4, pp. 356–366, Dec. 2013, doi: 10.1007/s12668-013-0112-7.

[4] A. A. M. Faudzi, Y. Sabzehmeidani, and K. Suzumori, "Application of Micro-Electro-Mechanical Systems (MEMS) as Sensors: A Review," Journal of Robotics and Mechatronics, vol. 32, no. 2, pp. 281–288, Apr. 2020, doi: 10.20965/jrm.2020.p0281.

[5] R. Bogue, "Recent developments in MEMS sensors: a review of applications, markets and technologies," Sensor Review, vol. 33, no. 4, pp. 300–304, Sep. 2013, doi: 10.1108/SR-05-2013-678.

[6] B. Padha, I. Yadav, S. Dutta, and S. Arya, "Recent Developments in Wearable NEMS/MEMS-Based Smart Infrared Sensors for Healthcare Applications," Oct. 24, 2023, American Chemical Society. doi: 10.1021/acsaelm.3c00860.

[7] Izhar, X. Zhao, H. Tavakkoli, W. Xu, and Y. K. Lee, "Performance Improvement of Integrated MEMS Temperature, Humidity, and Air Velocity Sensors for Application in Smart Buildings," IEEE Trans Electron Devices, vol. 71, no. 3, pp. 2064–2071, Mar. 2024, doi: 10.1109/TED.2024.3353147.

[8] Z. Stanimirovic and I. Stanimirovic, "Pt Resistive Film Sensors," in 2019 IEEE 31st International Conference on Microelectronics (MIEL), IEEE, Sep. 2019, pp. 145–148. doi: 10.1109/MIEL.2019.8889625.

[9] W. Tomboza, R. Cotillard, N. Roussel, M. C. P. Huy, G. Bouwmans, and G. Laffont, "Characterization of femtosecond laser micromachined fiber in-line pressure sensor for simultaneous measurement of high temperature and pressure," in Optica Advanced Photonics Congress 2022, Washington, D.C.: Optica Publishing Group, 2022, p. BTh2A.3. doi: 10.1364/BGPPM.2022.BTh2A.3.

[10] W. Sui, T. Kaisar, H. Wang, Y. Wu, J. Lee, H. Xie, and P. Feng, "Micromachined Thin Film Ceramic PZT Multimode Resonant Temperature Sensor," *IEEE Sens J*, vol. 24, no. 6, pp. 7273–7283, Mar. 2024, doi: 10.1109/JSEN.2023.3294125.

[11] H. Qian et al., "A High Sensitivity Temperature Sensor Using High-Q NS-SAW Resonator," in 2022 Joint Conference of the European Frequency and Time Forum and IEEE International Frequency Control Symposium (EFTF/IFCS), IEEE, Apr. 2022, pp. 1–4. doi: 10.1109/EFTF/IFCS54560.2022.9850684.

[12] X. Q. Bao, W. Burkhard, V. V. Varadan, and V. K. Varadan, "SAW Temperature Sensor and Remote Reading System," in IEEE 1987 Ultrasonics Symposium, IEEE, 1987, pp. 583–586. doi: 10.1109/ULTSYM.1987.199024.

[13] K.-H. Chiu, H.-R. Chen, and S. R.-S. Huang, "High-Performance Film Bulk Acoustic Wave Pressure and Temperature Sensors," *Jpn J Appl Phys*, vol. 46, no. 4R, p. 1392, Apr. 2007, doi: 10.1143/JJAP.46.1392.

[14] S. W. Wenzel and R. M. White, "A multisensor employing an ultrasonic Lamb-wave oscillator," IEEE Trans Electron Devices, vol. 35, no. 6, pp. 735–743, Jun. 1988, doi: 10.1109/16.2525.

[15] A. Nastro, M. Baù, M. Ferrari, L. Rufer, S. Basrour, and V. Ferrari, "Cell Alignment in Aqueous Solution Employing a Flexural Plate Wave Piezoelectric MEMS Transducer," IEEE Access, vol. 11, pp. 130755–130762, 2023, doi: 10.1109/ACCESS.2023.3333694.

[16] M. Reusch, K. Holc, A. Zukauskaite, V. Lebedev, N. Kurz, and O. Ambacher, "Flexural plate wave sensors with buried IDT for sensing in liquids," in 2017 IEEE SENSORS, IEEE, Oct. 2017, pp. 1–3. doi: 10.1109/ICSENS.2017.8234418.

[17] A. Nastro, L. Rufer, M. Ferrari, S. Basrour, and V. Ferrari, "Piezoelectric Micromachined Acoustic Transducer with Electrically-Tunable Resonant Frequency," in 2019 20th International Conference on Solid-State Sensors, Actuators and Microsystems & Eurosensors XXXIII (TRANSDUCERS & EUROSENSORS XXXIII), IEEE, Jun. 2019, pp. 1905–1908. doi: 10.1109/TRANSDUCERS.2019.8808488.

[18] Z. Yu, Y. Yue, Z. Liang, X. Zhao, F. Li, W. Peng, Q. Zhu and Y. He, "Physical Sensors Based on Lamb Wave Resonators", Micromachines (2024), 15, 1243. https://doi.org/10.3390/mi15101243.

[19] P. Kropelnicki et al., "CMOS-compatible ruggedized high-temperature Lamb wave pressure sensor," Journal of Micromechanics and Microengineering, vol. 23, no. 8, Aug. 2013, doi: 10.1088/0960-1317/23/8/085018.

[20] H. Jia, R. Duhamel, J.-F. Manceau, M. de Labachelerie, and F. Bastien, "Improvement of Lamb waves sensors," Sens Actuators A Phys, vol. 121, no. 2, pp. 321–326, Jun. 2005, doi: 10.1016/j.sna.2005.02.014.

[21] B. Cunningham, M. Weinberg, J. Pepper, C. Clapp, R. Bousquet, B. Hugh, R. Kant, C. Daly, E. Hauser, "Design, fabrication and vapor characterization of a microfabricated flexural plate resonator sensor and application to integrated sensor arrays," Sens Actuators B Chem, vol. 73, no. 2–3, pp. 112–123, Mar. 2001, doi: 10.1016/S0925-4005(00)00664-X.

[22] S. Bertelli, A. Nastro, M. Ferrari, M. Baù, and V. Ferrari, "Simulation and Experimental Validation of a Flexural Plate Wave Piezoelectric MEMS Transducer," in 2024 IEEE Sensors Applications Symposium (SAS), IEEE, Jul. 2024, pp. 1–6. doi: 10.1109/SAS60918.2024.10636618.